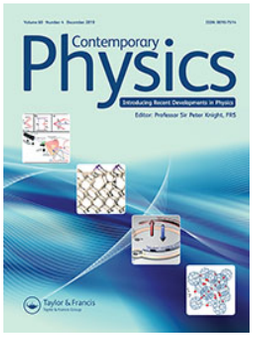

Contemporary Physics

ISSN: 0010-7514 (Print) 1366-5812 (Online) Journal homepage: https://www.tandfonline.com/loi/tcph20

Resolving starlight: a quantum perspective

Mankei Tsang

To cite this article: Mankei Tsang (2019) Resolving starlight: a quantum perspective, Contemporary Physics, 60:4, 279-298, DOI: 10.1080/00107514.2020.1736375

To link to this article: https://doi.org/10.1080/00107514.2020.1736375

Published online: 11 Mar 2020.

CONTEMPORARY PHYSICS
2020, VOL. 60, NO. 4, 279–298
https://doi.org/10.1080/00107514.2020.1736375

Taylor & Francis
Taylor & Francis Group

Resolving starlight: a quantum perspective

Mankei Tsang [a,b]

[a]Department of Electrical and Computer Engineering, National University of Singapore, Singapore, Singapore; [b]Department of Physics, National University of Singapore, Singapore, Singapore

ABSTRACT

The wave-particle duality of light introduces two fundamental problems to imaging, namely, the diffraction limit and the photon shot noise. Quantum information theory can tackle them both in one holistic formalism: model the light as a quantum object, consider any quantum measurement, and pick the one that gives the best statistics. While Helstrom pioneered the theory half a century ago and first applied it to incoherent imaging, it was not until recently that the approach offered a genuine surprise on the age-old topic by predicting a new class of superior imaging methods. For the resolution of two sub-Rayleigh sources, the new methods have been shown theoretically and experimentally to outperform direct imaging and approach the true quantum limits. Recent efforts to generalise the theory for an arbitrary number of sources suggest that, despite the existence of harsh quantum limits, the quantum-inspired methods can still offer significant improvements over direct imaging for subdiffraction objects, potentially benefiting many applications in astronomy as well as fluorescence microscopy.

ARTICLE HISTORY
Received 5 October 2019
Accepted 24 February 2020

KEYWORDS
Quantum optics; quantum information; optical imaging; statistics; superresolution; optical astronomy; fluorescence microscopy

1. Ingredients of the resolution problem: diffraction, photon shot noise, statistics

In 1879 Lord Rayleigh proposed a criterion of resolution for incoherent imaging in terms of two point sources [1]: the sources are said to be unresolvable if they are so close that their images, blurred by diffraction, overlap significantly. To quote Feynman [2], however, 'Rayleigh's criterion is a rough idea in the first place', and a better resolution can be achieved 'if sufficiently careful measurements of the exact intensity distribution over the diffracted image spot can be made'. Thus another limiting factor is the noise in the intensity measurement, with the photon shot noise being the most fundamental source. Because of the particle nature of light, each camera pixel can record its energy in discrete quanta only, and ordinary light sources, including starlight and fluorescence, introduce further randomness to the quantum measurements [3].

To incorporate noise in the definition of resolution, the theory of statistical inference offers a rigorous framework [4,5]. For example, a measure of resolution can be defined in terms of parameter estimation: given a blurry and noisy image of two point sources, how well can one estimate their separation [6–10]? Or it can be framed in terms of hypothesis testing: how well can one decide from the image whether there is one or two sources [11–14]? Such statistical treatments of resolution have garnered prominence in optical astronomy [6,12,15–19] and fluorescence microscopy [10,20–23], where the number of photons is limited and shot noise is part of life.

2. Quantum detection and estimation theory

Imaging has grown into a multidisciplinary problem that straddles optics, quantum mechanics, statistics, and signal processing. In a Herculean effort that began in the 1960s, Helstrom merged the subjects into a theory of quantum detection and estimation [24], which marked the beginning of quantum information theory. His aim was to determine the best measurement, out of the infinite possibilities offered by quantum mechanics, that optimises the performance of an inference task. For a given light source, the optimal performance then represents the most fundamental limit on the resolution, valid for any optics design that is allowed by quantum mechanics, as well as any computational technique in data postprocessing. In setting fundamental limits, Helstrom's theory plays a role for sensing and imaging not unlike the second law of thermodynamics for engines, ruling out unphysical superresolution methods in the same manner the second law rules out perpetual-motion machines.

CONTACT Mankei Tsang mankei@nus.edu.sg; https://blog.nus.edu.sg/mankei/

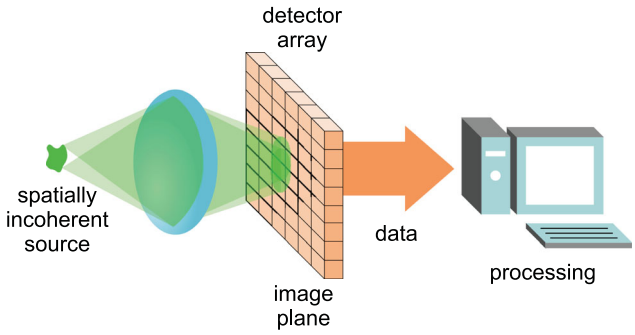

Figure 1. Basic setup of direct imaging.

The mathematics was formidable, but Helstrom managed to apply his theory to a few simple scenarios of incoherent imaging. For example, he studied the problem of locating an incoherent point source from far-field measurements [25], but the result was unsurprising: the quantum limit is close to the ideal performance of direct imaging, which measures the intensity on the image plane, as depicted by Figure 1. A more intriguing problem he studied was the decision between one or two incoherent sources [26]. Helstrom computed the mathematical form of the optimal measurement and the resulting error probabilities, but he did not propose an experimental setup or show how much improvement the optimal measurement could offer over existing imaging methods. Helstrom himself was quite pessimistic [26]: 'The optimum strategies required in order to attain the minimum error probabilities calculated here require the measurement of certain complicated quantum-mechanical projection operators, which, though possible in principle, cannot be carried out by any known apparatus'.

Unfortunately, in all the problems studied by Helstrom, the improvements predicted by his theory seemed modest at best, rendering the question of quantum limits academic. Quantum opticians turned their attention to nonclassical light sources [27–33], while classical opticians turned their attention to near-field microscopy [34,35], fluorescence control [34,36,37], and computational imaging [5]. Helstrom's work on incoherent imaging was all but forgotten.

Surprise came a few decades later. Applying quantum estimation theory to the problem of resolving two incoherent point sources, we recently discovered that substantial improvements via novel far-field measurements are indeed possible [38]. The theory has since been generalised for an arbitrary number of sources [39–45]. The implication is that, even for astronomy, where the sources are inaccessible, the new techniques can enhance the resolution beyond the limits of direct imaging – the de facto method developed by evolution for eons and honed by opticians for centuries. I present in the following an introduction to the breakthrough in Ref. [38], as well as the rapid theoretical [39–74] and experimental [75–86] advances that followed.

3. Rayleigh's curse

With two incoherent point sources, direct imaging, and photon shot noise, many studies have shown that their separation becomes harder to estimate if they violate Rayleigh's criterion [6–10]. The central tool used in those studies is the Fisher information, which sets general lower bounds called Cramér-Rao bounds on the parameter-estimation error [87]. The simplest Cramér-Rao bound (CRB) is

$$\mathrm{MSE}(\theta) \geq \mathrm{CRB}(\theta) \equiv \mathrm{FI}(\theta)^{-1}, \tag{1}$$

where MSE is the mean-square error of any unbiased estimator, θ is the unknown parameter, and $\mathrm{FI}(\theta)$ is the Fisher information; see Appendix 1 for precise definitions. The error can reach the Cramér-Rao bound in many situations, including an asymptotic limit where the sample size approaches infinity, the noise can be approximated as additive and Gaussian, and the maximum-likelihood estimator is used [87]. Thus, the Fisher information is a useful measure of the sensitivity of the experiment to the unknown parameter.

Assume one-dimensional paraxial imaging [88] for simplicity, as illustrated by Figure 2, and Poisson noise, which is an excellent approximation for both optical astronomy [18,19,89] and fluorescence microscopy [90]. The Fisher information becomes

$$\mathrm{FI}^{(\mathrm{direct})}(\theta) = C(\theta)N, \tag{2}$$

where θ here is the separation, N is the average photon number, and $C(\theta)$ is an N-independent prefactor that varies with θ. θ and $C(\theta)$ are dimensionless if θ is normalised in Airy units (1 Airy unit is roughly λ/N.A. where λ is the wavelength and N.A. is the numerical aperture, or λ/D for angular resolution, where D is the aperture diameter [90]). Equation (2) was earlier suggested by many as a fundamental measure of resolution for incoherent imaging [7–10].

The details of $C(\theta)$ depend on the point-spread function, but the general behaviour is as follows: If the sources are well separated relative to Rayleigh's criterion ($\theta \gg 1$), $C(\theta)$ is relatively constant, but when θ is close to Rayleigh's criterion or starts to violate it ($\theta \lesssim 1$), $C(\theta)$ decays to zero, causing the Cramér-Rao bound to blow up as $\theta \to 0$. In other words, there is a progressive penalty on the Fisher information for the violation of Rayleigh's criterion, as illustrated by Figure 3 for a Gaussian point-spread function. In Ref. [38], we called this

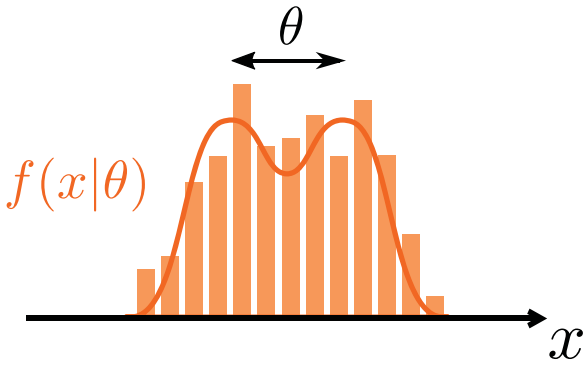

Figure 2. The image of two point sources (histogram) is blurred by diffraction and corrupted by photon shot noise. θ denotes the separation between the sources, $f(x \mid \theta)$ (solid curve) is the mean intensity, and x is the image-plane coordinate.

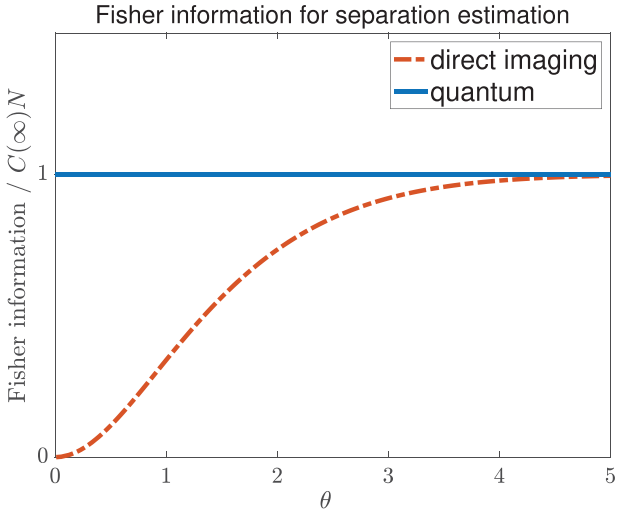

Figure 3. Fisher information for the estimation of the separation θ between two incoherent point sources, assuming a Gaussian point-spread function. With direct imaging, the information drops to zero for $\theta \to 0$, but the Helstrom information according to quantum estimation theory stays constant.

penalty Rayleigh's curse to distinguish it from Rayleigh's criterion – sub-Rayleigh sources are resolvable, but the more they violate Rayleigh's criterion, the harder it gets to estimate their separation.

4. Dispelling Rayleigh's curse

Rayleigh's curse happens if we measure the intensity on the image plane, but what if we allow any quantum measurement that may be sensitive to the phase as well? To find the quantum limit, we can use a quantum version of the Fisher information proposed by Helstrom [24], which sets an upper bound on the Fisher information for any measurement [91,92], as elaborated in Appendix 2. We found that the Helstrom information (HI) for the

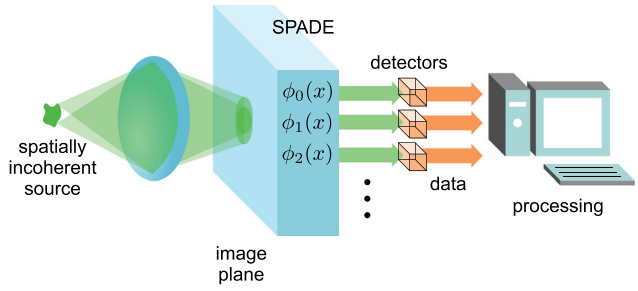

Figure 4. Basic setup of SPADE for incoherent imaging.

separation estimation problem is given by [38]

$$\mathrm{FI}(\theta) \leq \mathrm{HI}(\theta) = C(\infty)N. \tag{3}$$

Remarkably, $\mathrm{HI}(\theta)$ is constant regardless of the separation and completely free of Rayleigh's curse, as plotted in Figure 3.

The constant Helstrom information would be no surprise if it were simply a loose upper bound; the million-dollar question is whether one can find a measurement that attains the limit. Mathematical studies following Helstrom's work have shown in general that a quantum-limited measurement should exist, at least in the limit of infinite sample size [93,94]. The mathematics offers little clue to the experimental implementation, however, and finding one in quantum estimation theory is often a matter of educated guessing.

Luckily we found one. Assuming a Gaussian point-spread function, we found that sorting the light on the image plane in terms of the Hermite-Gaussian modes, followed by photon counting in each mode, can lead to a Fisher information given by [38]

$$\mathrm{FI}^{(\mathrm{SPADE})}(\theta) = C(\infty)N, \tag{4}$$

which attains the quantum limit and is free of Rayleigh's curse for all θ. Figure 4 illustrates the setup. We called the measurement spatial-mode demultiplexing with the acronym SPADE, to follow the convention of giving catchy acronyms to superresolution methods [36]. Numerical simulations have shown that SPADE combined with a judicious estimator can give an error very close to the quantum bound $1/\mathrm{HI}$ and substantially lower than that achievable by direct imaging [38,50]. Further studies have proposed measurements that work for other point-spread functions [38,46,53,55].

5. How SPADE works

To understand how SPADE can beat direct imaging and achieve the quantum limit, it is helpful to consider a simplified model of thermal light [38] that is valid for optical

frequencies and beyond, as described in the following. The model may sound heuristic, but it is possible to derive it from a quantum formalism by assuming a thermal quantum state [3], the paraxial optics model [95], and an 'ultraviolet' limit, as elaborated in Appendix 3.

Treat each photon on the image plane as a quantum particle with wavefunction $\psi(x)$, where x is the image-plane coordinate normalised with respect to the magnification factor [88]. Direct imaging corresponds to a measurement of its position, obeying the probability density

$$f(x) = |\psi(x)|^2, \tag{5}$$

by virtue of Born's rule. It is also possible to measure the particle in any other orthonormal basis $\{\phi_q(x) : q \in \mathbb{N}_0\}$, and the probability of finding the photon in the qth spatial mode is

$$g_q = \left| \int_{-\infty}^{\infty} \mathrm{d}x \phi_q^*(x)\psi(x) \right|^2. \tag{6}$$

For incoherent imaging, the wavefunction of each photon is $\psi(x - X)$, where ψ is determined by the point-spread function of a diffraction-limited imaging system and the displacement X depends on the position of the point source that emits the photon. Denoting the density of the incoherent sources as $F(X)$, X can be regarded as a random variable with $F(X)$ as its probability density. For direct imaging, the probability density on the image plane becomes

$$f(x) = \int_{-\infty}^{\infty} \mathrm{d}X |\psi(x - X)|^2 F(X), \tag{7}$$

which agrees with the classical theory of incoherent imaging [88]. In general, the probability of finding the photon in the $\phi_q(x)$ mode is

$$g_q = \int_{-\infty}^{\infty} \mathrm{d}X \left| \int_{-\infty}^{\infty} \mathrm{d}x \phi_q^*(x)\psi(x - X) \right|^2 F(X). \tag{8}$$

If we treat the arrivals of the photons at the spatial modes as a temporal Poisson process, then the photon counts integrated over time are independent Poisson random variables, each with mean and variance given by Ng_q, where N is the average photon number in all modes. For direct imaging, the photon statistics should be treated as a spatial Poisson process with mean intensity $Nf(x)$ [96].

Consider two point sources, one at $X = -\theta/2$ and one at $X = \theta/2$ such that $F(X) = [\delta(X - \theta/2) + \delta(X + \theta/2)]/2$. If their separation is deeply sub-Rayleigh ($\theta \ll 1$), the wavefunctions can be approximated as

$$\psi\left(x \pm \frac{\theta}{2}\right) \approx \psi(x) \pm \frac{\theta}{2} \frac{\partial \psi(x)}{\partial x}, \tag{9}$$

as depicted by Figure 5. If $\psi(x)$ is even, $\partial\psi(x)/\partial x$ is odd, and they can be regarded as two orthogonal modes. To

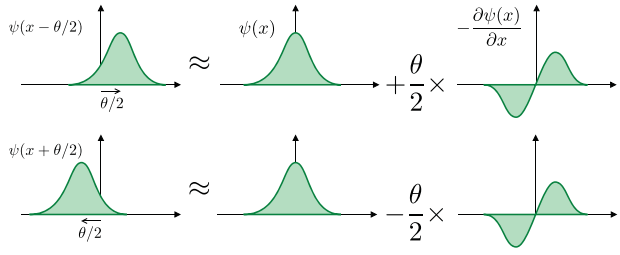

Figure 5. The wavefunction due to each point source can be decomposed in terms of the fundamental mode $\psi(x)$ and the derivative mode $-\partial\psi(x)/\partial x$ for $\theta \ll 1$. For incoherent point sources, the total energy in the derivative mode consists of the incoherent contributions from the sources ($\propto (\theta/2)^2 + (-\theta/2)^2 = \theta^2/2$). Thus the derivative mode contains the signal about θ, while the fundamental mode acts as a background noise.

the first order, the mean photon count in the fundamental $\psi(x)$ mode is insensitive to the parameter θ, while the mean count in the derivative mode is the incoherent sum of the contributions from the two sources, or $\propto (\theta/2)^2 + (-\theta/2)^2 = \theta^2/2$. If the sources were coherent and in-phase instead, their contributions to the derivative mode would cancel each other, leading to a much reduced signal [97]. In other words, the incoherence plays a key role in retaining a significant signal in the first order, and SPADE can extract this signal by measuring the derivative mode.

Another reason that SPADE can outperform direct imaging has to do with the fundamental mode $\psi(x)$. It contains little signal, but it overlaps spatially with the derivative mode and contributes a background to the spatial intensity measured by direct imaging, increasing the variances of the photon counts at each pixel. By projecting the fundamental mode into a different channel, SPADE filters out this background noise and substantially improves the signal-to-noise ratio.

The heuristic discussion so far can be made more rigorous by considering the Fisher information and the Cramér-Rao bounds. Assume that the object distribution $F(X \,|\, \theta)$ and therefore $f(x \,|\, \theta)$ and $g_q(\theta)$ depend on θ. For the spatial Poisson process from direct imaging, the Fisher information is [96]

$$\mathrm{FI}^{(\mathrm{direct})}(\theta) = N \int_{-\infty}^{\infty} \mathrm{d}x \frac{1}{f(x \,|\, \theta)} \left[\frac{\partial f(x \,|\, \theta)}{\partial \theta} \right]^2. \tag{10}$$

For separation estimation with $\theta \ll 1$,

$$f(x \,|\, \theta) \approx |\psi(x)|^2 + \frac{\theta^2}{8} \frac{\partial^2 |\psi(x)|^2}{\partial x^2}. \tag{11}$$

The denominator in Equation (10) approaches $|\psi(x)|^2$ as $\theta \to 0$, meaning that the fundamental mode is the major noise contributor, and the Fisher information approaches

zero as $\theta \to 0$. For discrete Poisson variables on the other hand, the Fisher information is

$$\mathrm{FI}(\theta) = N \sum_q \frac{1}{g_q(\theta)} \left[\frac{\partial g_q(\theta)}{\partial \theta}\right]^2. \qquad (12)$$

For separation estimation, as long as $\phi_1(x)$ is orthogonal to $\psi(x)$ and has significant overlap with the derivative mode, $g_1(\theta) \propto \theta^2$ for $\theta \ll 1$, leading to a nonzero $[\partial g_1(\theta)/\partial\theta]^2/g_1(\theta)$ as $\theta \to 0$.

To summarise, SPADE relies on the subtle interplay between the coherence induced by diffraction, the incoherence of the sources, and the signal-dependent nature of photon shot noise. It would have been difficult to discover such a fortuitous possibility via conventional wisdom alone, but quantum estimation theory – and quantum information theory in general – have the advantage of being oblivious to conventional wisdom. The mathematics may look daunting, but it can sometimes give rise to new physics beyond our imagination.

6. Implementations of SPADE

To implement SPADE, different spatial modes should be coupled into physically separate channels before detection. This in principle requires only linear optics [98], but the most efficient implementation remains unclear. Many methods have been proposed and demonstrated, particularly for the purpose of mode-division multiplexing in optical communication [33]. Here I highlight a few methods that have been experimentally demonstrated for the two-point resolution problem.

6.1. Interferometry

Nair proposed an interferometer called SLIVER (superlocalization via image-inversion interferometry) that can in principle achieve a quantum-limited Fisher information for $\theta \to 0$ and any even point-spread function [46]. Although image-inversion interferometry has earlier been proposed and demonstrated to combat atmospheric turbulence for astronomy [99] and to achieve a modest resolution improvement for general confocal microscopy [100–103], its extraordinary precision for sub-Rayleigh resolution was hitherto not recognised.

The setup, depicted by Figure 6, consists of a two-arm interferometer with spatial inversion in one arm. The inversion can be implemented via mirrors, lenses, or a Dove prism for example. As a result of the inversion and the interference at the second beamsplitter, all the even modes on the image plane are routed to one output port while the odd modes are routed to the other port. Hence, the fundamental mode $\psi(x)$, as long as it is even, is separated from the odd derivative mode, which is detected at

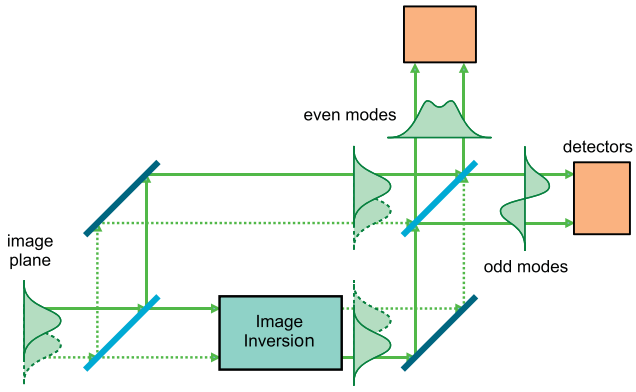

Figure 6. An image-inversion interferometer. Through the inversion and the interference, the even modes are coupled to one port while the odd modes are coupled to the other port.

the other port. Tang, Durak, and Ling reported a proof-of-concept demonstration of SLIVER [75], although their reported errors were not close to the quantum limit. Larson and coworkers recently reported a common-path configuration of the interferometer that may be more stable [104].

SLIVER works best for sub-Rayleigh separations but is suboptimal for larger separations. A variant of SLIVER called pix-SLIVER replaces the detectors by detector arrays and can work better for larger separations [48]. Another way to generalise SLIVER is to think of image inversion as a special case of fractional Fourier transform (FRFT). A tree of FRFT interferometers, with the image-inversion interferometer at its root, can sort the Hermite-Gaussian modes and implement SPADE [105]. The interferometer-tree concept can be generalised to sort in any other basis if appropriate mode-dependent phases can be introduced [106,107].

Along this direction, Hassett and coworkers demonstrated a Michelson interferometer with variable FRFT in one arm and used it to infer the Hermite-Gaussian-mode spectrum g_q of a shifted Gaussian beam [82]. They suggested that the setup could be useful for estimating sub-Rayleigh separations, although its statistical performance remains to be studied. In another work, Zhou and coworkers demonstrated a binary radial-mode sorter that is also based on FRFT interferometry and used it to enhance the estimation of the axial separation between two sources [83].

6.2. SPLICE

Tham, Ferretti, and Steinberg proposed an elegant setup called SPLICE (super-resolved position localisation by inversion of coherence along an edge) to capture the derivative mode [76]. SPLICE consists of a phase plate that introduces a π phase shift to half of the image plane

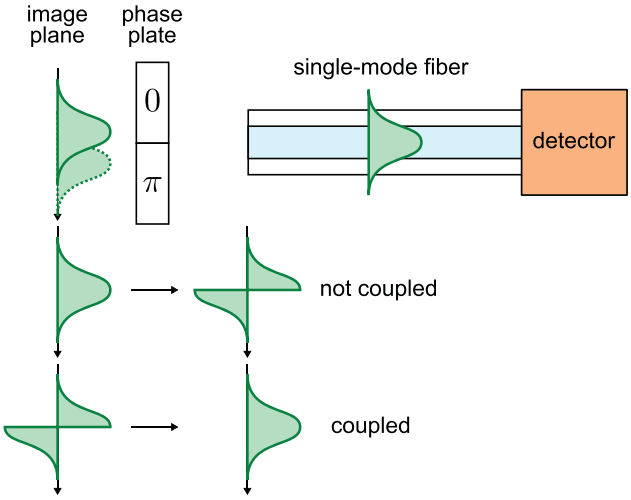

Figure 7. Setup and principle of SPLICE [76]. The phase plate introduces a π phase shift to half of the image plane relative to the other half. Only the odd mode that has been converted by the phase plate to the fiber mode is coupled into the fiber and detected.

and a single-mode fiber, as illustrated by Figure 7. An odd mode on the image plane is thus coupled into the fiber and detected, while all other modes orthogonal to it are rejected by the fiber. Despite the imperfect match between the odd mode and the derivative mode, Tham and coworkers were still able to demonstrate a mean-square error around five times the quantum bound and a significant improvement over direct imaging [76].

The use of phase plates is, of course, routine in phase-contrast microscopy [88,108], while the use of a half-plane π-phase plate specifically also has a long history in coherent imaging [108,109]. The important distinctions here are that we are dealing with incoherent sources, the phase plate is placed at the image plane, and there is a fiber that performs judicious spatial-mode selection.

6.3. Holograms

A hologram is capable of performing a spatial matched filter, and it can be designed such that the diffracted intensities at specific points in the far field are proportional to the modal spectrum g_q [88,110]. The use of such a hologram for separation estimation was demonstrated by Paúr and coworkers [77]. Their reported mean-square errors were around twice the quantum bound, but it is important to note that they scaled the quantum bound with respect to the diffracted photon number, not the photon number before the hologram, meaning that the result did not take into account the low diffraction efficiency of their hologram. Efficient SPADE is possible with multiple holograms, however [33].

6.4. Point-spread-function shaping

In the context of direct imaging, the approximation given by Equation (11) for $\theta \ll 1$ leads to

$$\mathrm{FI}^{(\mathrm{direct})} \approx \frac{N\theta^2}{16}\int_{-\infty}^{\infty} \mathrm{d}x \frac{[\partial^2|\psi(x)|^2/\partial x^2]^2}{|\psi(x)|^2 + (\theta^2/8)\partial^2|\psi(x)|^2/\partial x^2}. \quad (13)$$

It is often assumed [8,9] that this can be approximated by

$$\mathrm{FI}^{(\mathrm{direct})} \approx \frac{N\theta^2}{16}\int_{-\infty}^{\infty} \mathrm{d}x \frac{1}{|\psi(x)|^2}\left[\frac{\partial^2|\psi(x)|^2}{\partial x^2}\right]^2, \quad (14)$$

which scales quadratically with θ. This is indeed true if $|\psi(x)|^2$ is Gaussian, but it turns out that the integral in Equation (14) may not converge if $|\psi(x)|^2$ has zeros, and one must go back to Equation (13), which can give a linear scaling of $\mathrm{FI}^{(\mathrm{direct})}$ with θ instead. Paúr and coworkers exploited this phenomenon by introducing a signum phase mask at the pupil plane of a direct-imaging system, changing $\psi(x)$ from a Gaussian to an odd function with a zero in the middle [81]. Although the resulting Fisher information still approaches zero for $\theta \to 0$, they were able to demonstrate a significant improvement of the estimation accuracy with a simple change. Further experiments along the same line for spectroscopy have recently been reported [84].

6.5. Heterodyne

Given the experimental difficulties of performing efficient SPADE, a seemingly appealing alternative is to perform heterodyne detection of the derivative mode by interfering the light with a shaped reference beam on a detector, as demonstrated by Yang and coworkers [78]. It was later found, however, that the homodyne or heterodyne Fisher information still suffers from Rayleigh's curse for weak thermal light [54]. This can be attributed to the constant vacuum noise that plagues a heterodyne or homodyne detection regardless of the signal, compared with the Poisson variance that reduces with the signal for photon counting. A similar problem was discovered earlier in the context of stellar interferometry [111,112]. The surprisingly poor performance of heterodyne detection demonstrates the importance of analysing a measurement using rigorous quantum optics as well as statistics, even when dealing with classical light, to ensure an acceptable statistical performance.

6.6. Sum-frequency generation

Donohue and coworkers implemented SPADE in the time or frequency domain for estimating the separation between optical pulses via an interesting nonlinear-optical technique: sum-frequency generation [79]. If the light is combined with a strong local-oscillator pulse in a second-order nonlinear medium with the right phase matching, the Hamiltonian of the sum-frequency generation is the same as that of linear optics [113], and a temporal or spectral mode projection can be implemented if the local oscillator has the desired mode shape and the up-converted signal is measured. While the efficiency of their measurement was only 0.7%, the principle was clearly demonstrated in their experiment.

6.7. Two-photon measurement

Last but not the least, I should mention an even more radical proposal by Parniak and coworkers, which uses a two-photon measurement to estimate the centroid and the separation of two sources simultaneously near the quantum limit [80]. Its applicability to usual light sources is questionable, but it demonstrates the fact that our model of linear optics and Poisson statistics does not encompass all the possibilities offered by quantum mechanics, and there exist multiphoton measurements that can offer advantages in multiparameter estimation, at least in principle.

7. Extended sources

7.1. Estimation of the second moment

While the two-point problem is historic and significant, it has rather limited applications, and the important next step is to apply the concepts developed so far to more general objects. Suppose now that the number of point sources is arbitrary, and the object intensity is given in general by $F(X)$. Similar to the sub-Rayleigh approximation earlier, here I focus on a subdiffraction regime where the object width around $X = 0$, defined as Δ, is much smaller than the width of the point-spread function, or $\Delta \ll 1$. Otherwise, $F(X)$ is assumed to be unknown to the experimenter. Similar to Equation (9), the photon wavefunction due to each point X within the object can be approximated as

$$\psi(x - X) \approx \psi(x) - X\frac{\partial\psi(x)}{\partial x}. \tag{15}$$

Summing the incoherent contributions from all the points via Equation (8), the mean photon count in the derivative mode $\phi_1(x) \propto \partial\psi(x)/\partial x$ is

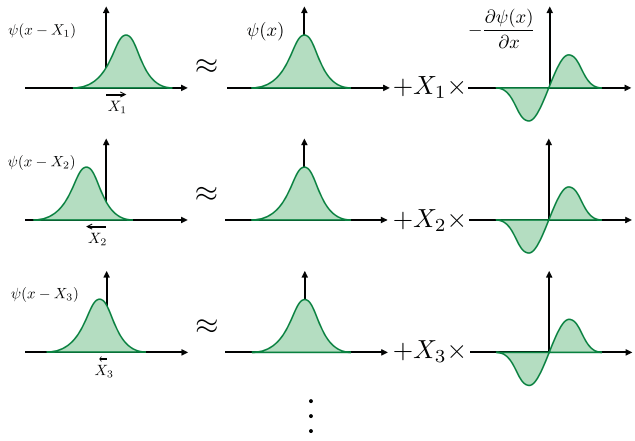

Figure 8. The wavefunction due to each point source can be decomposed in terms of the fundamental mode $\psi(x)$ and the derivative mode $-\partial\psi(x)/\partial x$ for $|X| \ll 1$. For multiple incoherent point sources, the total energy in the derivative mode consists of the incoherent contributions from the sources ($\propto X_1^2 + X_2^2 + X_3^2 + \ldots$ for equally bright sources). In other words, the energy is proportional to the second moment of the source distribution.

$$Ng_1 \approx Nc_1^2 \int_{-\infty}^{\infty} \mathrm{d}XX^2F(X), \tag{16}$$

where c_1 is a constant and $\int_{-\infty}^{\infty} \mathrm{d}XX^2F(X)$ is the second moment of $F(X)$. Figure 8 illustrates this concept for multiple point sources. Thus we can expect SPADE to enhance the estimation of the second moment for any subdiffraction object in the same way it enhances the two-point resolution. As the second moment can be related to the width of $F(X)$, it should not be surprising that SPADE can also enhance the estimation of the object size [39,41].

7.2. Even moments

To go another step further, let us expand $\psi(x - X)$ up to the qth order. It is more convenient to work in the spatial frequency domain, as defined by

$$\psi(x) \to \Psi(k) = \frac{1}{\sqrt{2\pi}} \int_{-\infty}^{\infty} \mathrm{d}x\psi(x) \exp(-ikx), \tag{17}$$

which leads to

$$\psi(x - X) \to \exp(-ikX)\Psi(k) \approx \sum_{p=0}^{q} \frac{(-ikX)^p}{p!}\Psi(k). \tag{18}$$

A natural orthonormal basis that includes the fundamental mode $\psi(x) \to \Psi(k)$ and the derivative mode

$-\partial\psi(x)/\partial x \to -ik\Psi(k)$ can be defined as [53]

$$\left\{\phi_q(x) \to \Phi_q(k) = (-i)^q b_q(k)\Psi(k) : q \in \mathbb{N}_0\right\}, \quad (19)$$

where $\{b_q(k)\}$ are the orthogonal polynomials obtained by applying the Gram-Schmidt process [114] to monomials $\{1, k, k^2, \ldots\}$ with respect to the weighted inner product [115]

$$\langle u(k), v(k)\rangle \equiv \int_{-\infty}^{\infty} \mathrm{d}k|\Psi(k)|^2 u^*(k)v(k), \quad (20)$$

leading to $\langle b_q(k), b_p(k)\rangle = \int_{-\infty}^{\infty} \mathrm{d}k\Phi_q^*(k)\Phi_p(k) = \delta_{qp}$. Appendix 4 gives a brief review of the Gram-Schmidt process. The basis $\{\phi_q(x)\}$ is called the point-spread-function-adapted basis [53], or the PAD basis for short [40]. For example, if $|\Psi(k)|^2$ is Gaussian, then $\{b_q(k)\}$ are the Hermite polynomials. An important property of $b_q(k)$ that follows from the Gram-Schmidt process is that $\langle b_q(k), k^p\rangle = 0$ if $p < q$. The overlap function in Equation (8) becomes

$$\int_{-\infty}^{\infty} \mathrm{d}x\phi_q^*(x)\psi(x - X)$$

$$\approx \sum_{p=0}^{q} \frac{(-iX)^p}{p!} \int_{-\infty}^{\infty} \mathrm{d}k\Phi_q^*(k)\Psi(k)k^p \quad (21)$$

$$= \sum_{p=0}^{q} \frac{(-iX)^p}{p!} i^q \left\langle b_q(k), k^p\right\rangle = c_q X^q, \quad (22)$$

where c_q is a real constant. In other words, $\Phi_q(k)$ is orthogonal to all the terms in Equation (18) except the last qth-order term (and the neglected higher-order terms). The mean photon count given by Equation (8) becomes

$$Ng_q \approx Nc_q^2 \int_{-\infty}^{\infty} \mathrm{d}X X^{2q} F(X). \quad (23)$$

Similar to the relation between the derivative mode and the second moment, each PAD mode can access an even moment while rejecting the background noise from all the lower moments [40]. Hence, SPADE with respect to the PAD basis can be expected to enhance the estimation of all even moments.

If $\psi(x)$ is Gaussian, the PAD basis becomes the Hermite-Gaussian basis, and its sensitivity to even moments was noted in Refs. [39,78]. The general PAD basis was proposed in Refs. [53,55] for the two-point problem and applied to general imaging in Refs. [40,43,44]. The use of SPLICE for moment estimation was recently proposed by Bonsma-Fisher and coworkers [45].

7.3. Error analysis

Define the moment parameters as

$$\theta_\mu = \int_{-\infty}^{\infty} \mathrm{d}X X^\mu F(X), \quad (24)$$

where $\mu \in \mathbb{N}$ denotes the moment order. Appendix 5 introduces the multiparameter-estimation theory in more detail. The mean and variance of the photon count n_q in each PAD mode is

$$Ng_q \approx Nc_q^2\theta_{2q}, \quad (25)$$

so the estimator $\check{\theta}_{2q} = n_q/(Nc_q^2)$ is approximately unbiased, and the mean-square error is [39,40,44]

$$\mathrm{MSE}_{2q}^{(\mathrm{SPADE})} \approx \frac{\theta_{2q}}{Nc_q^2} = \frac{O(\Delta^{2q})}{N}, \quad (26)$$

where the subscript $2q$ denotes the error for the θ_{2q} parameter, the big-O notation denotes terms on the order of the argument, and $\theta_\mu = O(\Delta^\mu)$. For direct imaging on the other hand, the Cramér-Rao bound for any moment is [39,40,44]

$$\mathrm{MSE}_\mu^{(\mathrm{direct})} \geq \mathrm{CRB}_\mu^{(\mathrm{direct})} = \frac{O(1)}{N}, \quad (27)$$

so SPADE can achieve much lower errors for the even moments in the $\Delta \ll 1$ subdiffraction regime. The exact Cramér-Rao bounds for both SPADE and direct imaging, as well as the unbiased estimators to achieve them, have been derived recently in Ref. [44] via semiparametric methods and are consistent with the approximate results here.

As large as the enhancement seems, the signal-to-noise ratio (SNR), defined as

$$\mathrm{SNR}_\mu \equiv \frac{\theta_\mu^2}{\mathrm{MSE}_\mu}, \quad (28)$$

offers a more sobering perspective, as the signal $\theta_\mu^2 = O(\Delta^{2\mu})$ is an even smaller number. For SPADE and even moments, the SNR turns out to be equal to the mean photon count in a PAD mode, or

$$\mathrm{SNR}_{2q}^{(\mathrm{SPADE})} \approx Ng_q = NO(\Delta^{2q}), \quad (29)$$

which decreases for smaller Δ and higher moments. The degradation of the SNR can be attributed to the inherently low efficiency of a subdiffraction source coupling into a higher-order mode. While this shows that SPADE

has its own limitations, the fact remains that direct imaging is even worse, with a SNR given by

$$\mathrm{SNR}_{\mu}^{(\mathrm{direct})} = NO(\Delta^{2\mu}), \tag{30}$$

which is $NO(\Delta^{4q})$ for $\mu = 2q$. With enough photons, the enhancements offered by SPADE can still be useful, especially for the lower moments.

7.4. Odd moments

To estimate an odd moment, consider projections into the pair of so-called iPAD modes

$$\phi_q^{(\pm)}(x) = \frac{\phi_q(x) \pm \phi_{q+1}(x)}{\sqrt{2}}, \tag{31}$$

which result from the interference of two adjacent PAD modes [40]. It makes intuitive sense that, if each ϕ_q mode is sensitive to the $2q$th moment, then a superposition of two adjacent PAD modes should be sensitive to an odd moment in-between. Expanding $\psi(x - X)$ up to the $(q + 1)$th order and following the same steps as Equations (21) and (22), the overlap function becomes

$$\int \mathrm{d}x \phi_q^{(\pm)*}(x)\psi(x - X) \approx \frac{1}{\sqrt{2}}\left(c_q X^q \pm c_{q+1}X^{q+1}\right), \tag{32}$$

where $|\Psi(k)|^2$ is assumed to be even such that $\{b_q(k)\}$ are alternatively even and odd, leading to $\langle b_q(k), k^{q+1}\rangle = 0$. Let the output counts be $n_q^{(\pm)}$. The mean counts are

$$Ng_q^{(\pm)} \approx \frac{N}{2}\int \mathrm{d}X \left(c_q X^q \pm c_{q+1}X^{q+1}\right)^2 F(X). \tag{33}$$

Subtracting one count by the other, the mean is

$$N(g_q^{(+)} - g_q^{(-)}) \approx 2Nc_q c_{q+1}\theta_{2q+1}, \tag{34}$$

so an estimator of the odd moment θ_{2q+1} can be constructed as $\check{\theta}_{2q+1} = (n_q^{(+)} - n_q^{(-)})/(2Nc_q c_{q+1})$. The variance of $n_q^{(+)} - n_q^{(-)}$ is $N(g_q^{(+)} + g_q^{(-)}) \approx N(c_q^2\theta_{2q} + c_{q+1}^2\theta_{2q+2})$, so the mean-square error becomes [39,40]

$$\mathrm{MSE}_{2q+1}^{(\mathrm{SPADE})} \approx \frac{1}{4N}\left(\frac{\theta_{2q}}{c_{q+1}^2} + \frac{\theta_{2q+2}}{c_q^2}\right) = \frac{O(\Delta^{2q})}{N}, \tag{35}$$

and the SNR becomes

$$\mathrm{SNR}_{2q+1}^{(\mathrm{SPADE})} \approx \frac{N(g_q^{(+)} - g_q^{(-)})^2}{g_q^{(+)} + g_q^{(-)}} = NO(\Delta^{2q+2}). \tag{36}$$

For the first moment ($q = 0$), the error is the same as the well known $O(1)/N$ error for point-source localisation [15,20]. For the third and higher moments, however, there is significant enhancement over direct imaging. Note also that $n_q^{(+)} + n_q^{(-)}$ can give information about the even moments as well.

7.5. Fourier object analysis via moments

The moments can be used in a (generalized) Fourier analysis that may be more familiar to opticians [5]. Suppose that $F(X)$ can be expanded as

$$F(X) = \sum_{\mu=0}^{\infty} \tilde{F}_\mu h_\mu(X)G(X), \tag{37}$$

where $G(X)$ is a nonnegative reference density, $\{h_\mu(X) = \sum_{\nu=0}^{\mu} H_{\mu\nu}X^\nu : \mu \in \mathbb{N}_0\}$ are orthogonal polynomials that satisfy

$$\int_{-\infty}^{\infty} \mathrm{d}X G(X)h_\mu(X)h_\nu(X) = \delta_{\mu\nu}, \tag{38}$$

and $\{\tilde{F}_\mu\}$ are generalised Fourier coefficients. Each $h_\mu(X)$ has μ distinct zeros on the support of $G(X)$ [115], so each $h_\mu(X)G(X)$ can be regarded as a wavelet that exhibits localised oscillations. The Fourier coefficients can be expressed as

$$\tilde{F}_\mu = \int \mathrm{d}X h_\mu(X)F(X) = \sum_{\nu=0}^{\mu} H_{\mu\nu}\theta_\nu. \tag{39}$$

In other words, each Fourier coefficient of order μ can be reconstructed from moments up to order μ. Thus the number of accurately estimated moments can be regarded as a measure of resolution, and SPADE can help by bringing in more accurate moments and increasing the number of obtainable Fourier coefficients for a subdiffraction object.

With a finite number of moments or Fourier coefficients and no other prior information, the reconstruction of $F(X)$ is ill-posed and requires regularisation [5]. Many linear or nonlinear algorithms can be used, depending on the application [5].

7.6. Quantum limits

Through the Helstrom information, we have learned earlier that SPADE is optimal for estimating the separation of two point sources. References [25,39] show that direct imaging is close to optimal for locating a subdiffraction object with a known shape, while Ref. [39] also shows that SPADE is close to optimal for estimating its size. Generalizing such results for arbitrary moments is much more difficult, as there are now an infinite number of parameters and an infinite number of spatial modes. Zhou and Jiang [43] showed essentially that any measurement should give a Fisher information that scales with Δ as

$$\mathrm{FI}_\mu = NO(\Delta^{-\mu_1}), \quad \mu_1 \le \mu, \tag{40}$$

where μ_1 is an integer. With the Cramér-Rao bound $\mathrm{MSE}_\mu \geq 1/\mathrm{FI}_\mu$, the SNR should scale as

$$\mathrm{SNR}_\mu \leq \theta_\mu^2 \mathrm{FI}_\mu = NO(\Delta^{\mu_2}), \quad \mu_2 \geq \mu, \tag{41}$$

where μ_2 is another integer. This means that, for a given μ, the SNR must decrease for smaller Δ, and the decrease is faster for higher μ. The best scaling with Δ is achieved at $\mu_1 = \mu_2 = \mu$, matching the scaling of the SPADE error given by Equation (26) for the even moments. Zhou and Jiang did not provide a tractable bound on the prefactor of Equation (40), however, so it remains a question whether SPADE is at all close to the quantum limit in absolute terms, or there may yet be superior measurements.

Using more standard quantum estimation theory, Ref. [42] proves a quantum limit given by

$$\mathrm{FI}_\mu \leq \mathrm{HI}_\mu \leq \mathrm{HI}'_\mu = NO(\Delta^{-2\lfloor \mu/2 \rfloor}), \tag{42}$$

where HI' is an absolute limit that does not depend on the measurement and can be approximated analytically or numerically. The scaling of $1/\mathrm{HI}'_\mu$ with Δ matches the errors of SPADE given by Equations (26) and (35), suggesting that SPADE is close to quantum-optimal for both even and odd moments, but a more quantitative comparison of the quantum limit with the SPADE performance remains to be done. A limit on the SNR is

$$\mathrm{SNR}_\mu \leq \theta_\mu^2 \mathrm{HI}'_\mu = NO(\Delta^{2\lceil \mu/2 \rceil}). \tag{43}$$

For a given subdiffraction object, Ref. [42] also shows that $\theta_\mu^2 \mathrm{HI}'_\mu$ must decay quickly with higher μ, meaning that higher moments are fundamentally more difficult to estimate.

8. Other generalisations

8.1. Unknown centroid

A crucial assumption in the preceding discussion is that the object is highly concentrated near a known coordinate $X = 0$, and the SPADE device is ideally aligned with $X = 0$. To put it the other way, Δ should be regarded as the object width plus any misalignment of SPADE with the object centroid, and misalignment can reduce the enhancement by increasing the effective Δ. As direct imaging can locate the centroid accurately, the misalignment can be minimised if the object of interest has been imaged before and its centroid is already known accurately, as is often the case in astronomy. Otherwise, some overhead photons should be used to locate the centroid first. Grace and coworkers found that, despite the overhead, SPADE can still offer significant enhancements of the two-point resolution over direct imaging with the same total photon number [67].

In principle, it turns out to be possible to estimate the centroid and the separation simultaneously at the quantum limit if a multiphoton measurement is performed, as demonstrated by Parniak and coworkers [56,80], but the applicability of their measurement to usual light sources is questionable.

8.2. Strong thermal light

While the model of weak thermal light and Poisson statistics works well for astronomical or fluorescent sources at optical frequencies, thermal sources at lower frequencies or scattered laser sources can exhibit super-Poisson statistics [3]. Nair computed the Helstrom information for separation estimation with the exact thermal state and also proposed variations of SPADE and SLIVER to approach it [48]. Lupo and Pirandola computed the quantum limit for the same problem but assumed arbitrary quantum states, including the thermal state as a special case [49]. Yang and coworkers studied the use of mode homodyne or heterodyne detection for the two-point problem and found that, although it is not competitive for weak thermal light, it can offer an enhancement over direct imaging for strong thermal light [54].

For radio and microwave frequencies, photon shot noise is negligible at typical temperatures, and heterodyne detection in any spatial-mode basis is quantum-optimal in the low-frequency limit [42, Appendix A2]. As amplitude measurements via antennas are already the standard detection method there and they are usually contaminated with substantial excess noise, the ideas here are not relevant to those frequencies unfortunately.

8.3. Two point sources with unequal brightnesses

Řeháček and coworkers studied the quantum limits and the optimal measurements for two point sources with unequal brightnesses [57,58]. They found that, while significant enhancements over direct imaging remain possible, the performance gets worse for unequal sources. In hindsight, this is perhaps not surprising, as moments up to the third are needed to fully parametrise unequal sources and the SNR for the third moment is fundamentally poorer. The use of SPLICE for this case was also studied by Bonsma-Fisher and coworkers [45], while the three-dimensional case was recently studied by Prasad [63].

8.4. More than two point sources

Bisketzi and coworkers [68] and Lupo et al. [69] recently proposed methods to compute the quantum limit to the

localisation of more than two point sources. Bisketzi and coworkers found numerically that, regardless of the number of sources, the Helstrom information matrix retains only two nonzero eigenvalues as the source separations approach zero. This result is complementary to – and consistent with – existing results on moment estimation [42,43], demonstrating the harsh quantum limits to imaging beyond centroid and size estimation. As the location parameters they considered are related nonlinearly to the moment parameters, the Helstrom information matrix transforms in a nontrivial way [116], and a more quantitative comparison of Ref. [68] with Refs. [42,43] will require further effort.

Lupo and coworkers also studied the achievability of the general quantum limit via interferometers [69]. More work remains to be done to ascertain whether their proposed interferometer design can be implemented without knowing the unknown parameters.

8.5. Excess detector noise

If the detectors are contaminated with excess noise besides photon shot noise, the estimation performance necessarily suffers. Len and coworkers studied the Fisher information of SPADE in the presence of such noise [73], while Lupo studied the quantum limits [74]. A fair comparison of these results with noisy direct imaging remains to be done, however. Considering that the ideal model of direct imaging assumes an infinitesimal pixel size, an infinite number of pixels, no excess noise, and perfect calibration of all pixels, imperfections in real life may well be even more detrimental to direct imaging.

8.6. Partially coherent sources

Larson and Saleh studied the separation estimation problem for two partially coherent sources and suggested that Rayleigh's curse would recur [64,66]. Their work has been challenged by Refs. [65,70,85], however. Reference [65] points out a few problems with Larson and Saleh's analysis, such as the use of a formula for the Helstrom information that becomes questionable for partially coherent sources. References [65,70,85] also show that SPADE can overcome the curse as long as the sources are not highly correlated, contrary to Larson and Saleh's claim. Another interesting work on this topic was done by Hradil and coworkers [72], who also used the questionable formula; see Appendix 3 for details. In any case, the debate is irrelevant to observational astronomy and fluorescence microscopy, where there is no sound reason to doubt the established model of spatially incoherent sources [89,90].

8.7. Two-dimensional imaging

Although I have so far focussed on imaging in one dimension for pedagogy, the same principles carry over to two dimensions. For two point sources, there are now two parameters for their vectoral separation. The quantum limits for the two parameters are the same as that for the one-dimensional case, and SPADE with respect to the transverse-electromagnetic (TEM) modes or a pair of SLIVER devices can still estimate the vectoral separation near the quantum limit [51]. For extended sources in two dimensions, a generalisation of the PAD and iPAD modes have been studied in Refs. [39,40,43], and quantum limits have been studied in Refs. [39,43].

8.8. Three-dimensional imaging

Reference [97] studies quantum limits to the three-dimensional localisation of one point source as well as two coherent sources using the full vectoral electromagnetics model (the discussion of incoherent sources there is flawed and superseded by Ref. [38]). In the context of the paraxial model on the other hand, the axial dimension requires special treatment [88]. For the axial localisation of one point source, Řeháček and coworkers demonstrated that direct imaging with a judicious defocus, a common technique in localisation microscopy [22,23], can attain the quantum limit [86]. Backlund, Shechtman, and Walsworth computed the quantum limit to the three-dimensional localisation of a point source using a scalar wave model and proposed special interferometers to achieve it [59]. Yu and Prasad [61–63] and Napoli and coworkers [60] studied the same problem but for two incoherent sources. Zhou and coworkers recently demonstrated a FRFT interferometer to enhance the estimation of the axial separation between two sources [83].

8.9. Spectroscopy

Donohue and coworkers demonstrated mode-selective measurements to enhance time and frequency estimation for incoherent optical pulses [79]. On a more mathematical level, the quantum model of a photon from incoherent sources coincides with that of a quantum probe subject to random displacements, as pointed out by Ref. [42], so noise spectroscopy with optomechanics or spin ensembles is another potential application of the theory [71,117].

8.10. Biased estimators

The simplest form of the Cramér-Rao bound is applicable to unbiased estimators only, and it turns out that biased estimators may violate it significantly [87]. For

example, the Cramér-Rao bound for separation estimation with direct imaging blows up to infinity as $\theta \to 0$, but the maximum-likelihood estimator, being biased for this problem, can still achieve a finite error for all θ [75,76,118]. For SPADE, the maximum-likelihood estimator can also violate the Cramér-Rao bound and give a vanishing error as $\theta \to 0$ [38]. Given these violations, one may wonder if the Cramér-Rao bound is meaningful outside the theoretical construct of asymptotic statistics [87] after all. The loophole can be fixed by using a Bayesian version of the Cramér-Rao bound [119] that is valid for any biased or unbiased estimator. Reference [50] shows that, from the Bayesian and minimax perspectives, there remains a significant performance gap between direct imaging and SPADE for separation estimation, even if biased estimators are permitted.

8.11. One-versus-two hypothesis testing

Another way of defining the two-point resolution is to consider the error probabilities of deciding whether there is one point source or two point sources with the same total brightness. As mentioned in Section 2, Helstrom performed a pioneering study of this problem using his quantum detection theory [26], but his proposed measurement depends on the separation in the two-source hypothesis, he did not suggest any experimental setup to realise it, and he did not show how much improvement it could offer. In the context of direct imaging, the problem was also studied in Refs. [11–14].

Coming in full circle, Lu and coworkers recently showed that the quantum limit to the hypothesis-testing problem is indeed a substantial improvement over direct imaging, and both SPADE and SLIVER can reach the quantum limit in the sub-Rayleigh regime, without knowing the separation in advance [52].

9. Comparison with other imaging techniques

In the wider context of imaging research, SPADE is but one of the countless superresolution proposals in the literature. It nonetheless possesses many unique advantages and avoids some common pitfalls of prior ideas, thanks to its firm footing in quantum optics and statistics. Its advantages over direct imaging and computational techniques have already been emphasised in previous sections, and here I highlight some other important or popular ideas in imaging and how SPADE compares.

9.1. Stellar interferometry

SPADE perhaps bears the most resemblance to stellar interferometry [89,99,120], as they are both examples of applying coherent optical processing to incoherent imaging. In particular, SLIVER resembles the folding and rotation-shearing interferometers in optical astronomy, the only difference being that the former is placed at the image plane and the latter usually at the pupil plane [99]. Conventional wisdom suggests, however, that the main advantage of stellar interferometry lies in its robustness against atmospheric turbulence [89,99,120]. To quote Goodman [89]:

> "The reader may well wonder why the Fizeau stellar interferometer, which uses only a portion of the telescope aperture, is in any way preferred to the full telescope aperture in this task of measuring the angular diameter of a distant object. The answer lies in the effects of the random spatial and temporal fluctuations of the earth's atmosphere ('atmospheric seeing') . . . It is easier to detect the vanishing of the contrast of a fringe in the presence of atmospheric fluctuations than it is to determine the diameter of an object from its highly blurred image.

Zmuidzinas [18] also suggested that 'the imperfect beam patterns of sparse-aperture interferometers extract a sensitivity penalty as compared with filled-aperture telescopes, even after accounting for the differences in collecting areas'. No work before ours recognised that interferometry can outperform direct imaging on statistical terms for diffraction-limited, filled-aperture telescopes.

Another use of stellar interferometry is to increase the baseline by coherently combining light from multiple apertures [120]. Our theory can also be applied to this multi-aperture scenario if we take the optical transfer function $\Psi(k)$ defined by Equation (17) to be the total aperture function for all the apertures. While conventional interferometer designs call for the interference of light from pairs of apertures [120] or the mimicking of image-formation optics [18,120], our theory offers the novel insight that demultiplexing the light in terms of the PAD or iPAD modes associated with $\Psi(k)$ can bring substantial advantages. This perspective generalises the recent studies on the quantum optimality of stellar interferometry [69,112,121,122].

Another idea that sounds similar to SLIVER is nulling interferometry [120], which was proposed for the specific purpose of exoplanet detection. The idea there is to remove the light from a bright star via destructive interference while leaving the light from a nearby planet intact, but its fundamental statistical performance in the subdiffraction regime has not been studied to our knowledge. It remains open questions whether nulling interferometry or similar ideas in astronomy turn out to perform similarly to SLIVER or SPADE, and how the quantum-inspired techniques and the quantum limits may benefit

important astronomical applications in practice, such as exoplanet detection.

9.2. Multiphoton coincidence

While modern stellar interferometers all rely on amplitude interference [120], also called $g^{(1)}$ measurements in quantum optics, the intensity interferometer by Hanbury Brown and Twiss – a $g^{(2)}$ measurement – deserves a mention as well, considering that it inspired the foundation of quantum optics [3] and is still being held in high regard by quantum opticians. In astronomy, however, the intensity interferometer has in fact been obsolete for decades because of its poor SNR [89,120]. It relies on the postselection of two-photon-coincidence events, which are much rarer than the one-photon events used in amplitude interferometry and therefore must give much less information in principle. For example, Davis and Tango reported an amplitude interferometer that obtained similar results to those from the intensity interferometer, using only ∼2% of the observation time [123]. For microscopy, the use of multiphoton coincidence has recently been demonstrated in some heroic experiments [124–127], but again its statistical performance needs to be studied more carefully. SPADE, on the other hand, is a $g^{(1)}$ measurement that relies on the much more abundant one-photon events without the need for coincidence detection and its statistical performance has been proved rigorously.

9.3. Electron microscopy and near-field microscopy

If the object is on a surface and accessible, then no technique can compete with electron microscopy, atomic force microscopy, and scanning-tunnelling microscopy in terms of resolution. Those techniques impose stringent requirements on the sample however, and that is why optical microscopy remains useful, especially for biological imaging, as it is able to image biological samples in a more natural environment and provide protein-specific contrast via fluorophore tagging.

In terms of optics, near-field techniques have not been successful because of the short depth of focus and other technical challenges [34]. In recent years, the use of plasmonics and metamaterials to enhance the near field [35] has also attracted immense interest in the academia, but the requirement of close proximity to the object and the impact of loss remain showstoppers in practice [128].

Being a far-field technique, SPADE is more compatible with biological imaging, not to mention its unique capability for astronomy and remote sensing. Unlike metamaterials, SPADE requires only low-loss optical components and there is no stringent requirement on their feature size, so fabrication is more straightforward.

Given the theoretical similarity between optical imaging and electron microscopy [8,9], the application of SPADE to the latter is possible in principle and indeed tantalising, but more research concerning its implementation for electrons needs to be done.

9.4. Superresolution fluorescence microscopy

Far-field superresolution techniques such as PALM and STED have been hugely successful in biological flouresence microscopy [34,36,37], but many of them rely on sophisticated control of the source emission, which introduces many other problems, such as the need for special fluorophores, slow speed in the case of PALM, and phototoxicity in the case of STED. SPADE, on the other hand, is a passive far-field measurement that can complement or supersede the superresolution techniques by extracting more information from the light or alleviating the need for source control. The combination of SPADE with microscope configurations, such as confocal and structured illumination [90], awaits further research.

9.5. Nonclassical light

The application of nonclassical light to sensing and imaging has been an active research topic in quantum optics for many decades [27–33]. It is now well known, however, that nonclassical light is extremely fragile against loss and decoherence [29,30], and any theoretical advantage can be easily lost in practice, not to mention that the efficient generation and detection of nonclassical light remain very challenging. More recent proposals, such as quantum illumination and quantum reading [31], apply to high-noise scenarios, but the achievable improvement turns out to be quite modest even in theory [129].

As SPADE works with classical light, linear optics, and photon counting, loss and other imperfections are not nearly as detrimental. If we are to believe that the second quantum revolution is near and applications using nonclassical resources will soon be widespread [130], then SPADE should be an even surer bet.

For astronomy, obviously the light sources cannot be controlled, but the use of entangled photons and quantum repeaters has been proposed to teleport photons in stellar interferometry and increase its baseline [131,132]. Unfortunately, quantum repeaters are nowhere near practical yet, and conventional linear optical devices remain the best option in the foreseeable future.

9.6. Superoscillation, amplification, postselection

There are so many other superresolution ideas that going through them all would not be feasible. I list here only a few more: superoscillation [133], amplification [134], and postselection [135]. They either require steep trade-offs with the SNR or have questionable statistics [136,137]. These examples once again demonstrate the importance of a rigorous analysis using quantum optics and statistics. It is important to keep in mind that superresolution is possible even with direct imaging and data processing, and it is ultimately limited by the SNR [5]. A superresolution technique is viable only if it can beat direct imaging on statistical terms.

10. Conclusion

Just as the design of engines must go beyond mechanics and consult thermodynamics, the design of optical sensing and imaging systems must go beyond electromagnetics and consult statistics. With the increasingly dominant role of photon shot noise in modern applications, quantum mechanics is also relevant. Quantum information theory can tackle all these subjects in one unified formalism, setting limits to what we can do, and also telling us how much further we can go. For incoherent imaging, it gives us the pleasant surprise that there is still plenty of room for improvement, and we just need to find a way to achieve it. We found one in the form of SPADE, which requires only low-loss linear optics and photon counting. While we started with the simple model of two point sources, we have since generalised the theory to deal with any subdiffraction object, showing that substantial improvements remain possible. The theoretical groundwork has been laid, proof-of-principle experiments have been done, and applications in astronomy and fluorescence microscopy can now be envisioned. Special-purpose applications that require only the low-order moments, such as two-point resolution and object-size estimation, should be the first to benefit, while more general imaging protocols will require further research.

Many open problems still remain. On the theoretical side, the exact quantum limits to general imaging and the optimal measurements to achieve them remain unclear. The theory for three-dimensional imaging and spectroscopy remains underdeveloped. On the practical side, an efficient implementation of SPADE at the right wavelengths is needed for applications. The performance of SPADE in the presence of atmospheric turbulence and other technical noises also needs to be assessed. Fortunately, adaptive optics [138], photodetectors [139], and photonics in general have become so good in recent years that we can be optimistic about reaching the quantum limits in the near future.

Acknowledgments

I am grateful to the seminal contributions of the authors of Refs. [38–86], especially the crucial roles of Ranjith Nair, Xiao-Ming Lu, and Shan Zheng Ang in our early papers. I also acknowledge useful discussions with Luis Sánchez-Soto, Jaroslav Řeháček, Zdeněk Hradil, Saikat Guha, and Cosmo Lupo in the course of writing this manuscript.

Disclosure statement

No potential conflict of interest was reported by the author(s).

Funding

This work is supported by the Singapore National Research Foundation under Project No. QEP-P7.

Notes on contributor

Mankei Tsang obtained his B.S. degrees in Electrical Engineering and Physics from UCLA in 2002 and his M.S. and Ph.D. degrees in Electrical Engineering from Caltech in 2004 and 2006, respectively. He held postdoctoral appointments with Demetri Psaltis at Caltech, with Jeffrey Shapiro and Seth Lloyd at MIT, and with Carlton Caves at the University of New Mexico. In 2011 he received the Singapore National Research Foundation Fellowship and moved to the National University of Singapore, where he is currently an Associate Professor at the Department of Electrical and Computer Engineering and the Department of Physics. His research interests include optics, superresolution, quantum measurement theory, and quantum information theory.

ORCID

Mankei Tsang http://orcid.org/0000-0001-7173-1239

References

[1] Rayleigh L. XXXI. Investigations in optics, with special reference to the spectroscope. Philos Mag Ser 5. 1879;8:261–274.
[2] Feynman RP, Leighton RB, Sands M. The Feynman lectures on physics. Vol. 1. Pasadena: California Institute of Technology; 2013. Chapter 30. Diffraction.
[3] Mandel L, Wolf E. Optical coherence and quantum optics. Cambridge: Cambridge University Press; 1995.
[4] den Dekker AJ, van den Bos A. Resolution: a survey. J Opt Soc Am A. 1997;14:547–557.
[5] de Villiers G, Roy Pike E. The limits of resolution. Boca Raton: CRC Press; 2016.
[6] Falconi O. Limits to which double lines, double stars, and disks can be resolved and measured. J Opt Soc Am. 1967;57:987–993.
[7] Tsai M-J, Dunn K-P. Performance limitations on parameter estimation of closely spaced optical targets using shot-noise detector model. Lincoln Laboratory, MIT; 1979. (Tech. rep.; ADA073462).
[8] Bettens E, Van Dyck D, den Dekker AJ, et al. Model-based two-object resolution from observations having counting statistics. Ultramicroscopy. 1999;77:37–48.

[9] Van Aert S, den Dekker AJ, Van Dyck D, et al. High-resolution electron microscopy and electron tomography: resolution versus precision. J Struct Biol. 2002;138:21–33.
[10] Ram S, Ward ES, Ober RJ. Beyond Rayleigh's criterion: A resolution measure with application to single-molecule microscopy. Proc Natl Acad Sci USA. 2006;103:4457–4462.
[11] Harris JL. Resolving power and decision theory. J Opt Soc Am. 1964;54:606–611.
[12] Acuna CO, Horowitz J. A statistical approach to the resolution of point sources. J Appl Stat. 1997;24:421–436.
[13] Shahram M, Milanfar P. Imaging below the diffraction limit: a statistical analysis. IEEE Trans Image Process. 2004;13:677–689.
[14] Shahram M, Milanfar P. Statistical and information-theoretic analysis of resolution in imaging. IEEE Trans Inform Theory. 2006;52:3411–3437.
[15] Farrell EJ. Information content of photoelectric star images. J Opt Soc Am. 1966;56:578–587.
[16] Lucy LB. Statistical limits to super resolution. Astron Astrophys. 1992;261:706.
[17] Lucy LB. Resolution limits for deconvolved images. Astron J (NY). 1992;104:1260–1265.
[18] Zmuidzinas J. Cramér–Rao sensitivity limits for astronomical instruments: implications for interferometer design. J Opt Soc Am A. 2003;20:218–233.
[19] Feigelson ED, Babu GJ. Modern statistical methods for astronomy. Cambridge: Cambridge University Press; 2012.
[20] Deschout H, Zanacchi FC, Mlodzianoski M, et al. Precisely and accurately localizing single emitters in fluorescence microscopy. Nat Methods. 2014;11:253–266.
[21] Chao J, Ward ES, Ober RJ. Fisher information theory for parameter estimation in single molecule microscopy: tutorial. J Opt Soc Am A. 2016;33:B36.
[22] von Diezmann A, Shechtman Y, Moerner WE. Three-dimensional localization of single molecules for super-resolution imaging and single-particle tracking. Chem Rev. 2017;117:7244–7275.
[23] Zhou Y, Handley M, Carles G, et al. Advances in 3D single particle localization microscopy. APL Photon. 2019;4:060901.
[24] Helstrom CW. Quantum detection and estimation theory. New York: Academic Press; 1976.
[25] Helstrom CW. Estimation of object parameters by a quantum-limited optical system. J Opt Soc Am. 1970;60:233–239.
[26] Helstrom CW. Resolution of point sources of light as analyzed by quantum detection theory. IEEE Trans Inform Theory. 1973;19:389–398.
[27] Kolobov MI. The spatial behavior of nonclassical light. Rev Mod Phys. 1999;71:1539–1589.
[28] Dowling JP. Quantum optical metrology – the low-down on high-N00N states. Contemp Phys. 2008;49:125–143.
[29] Demkowicz-Dobrzański R, Jarzyna M, Kołodyński J. Quantum limits in optical interferometry. In: Wolf E, editor. Progress in optics. Vol. 60. Amsterdam: Elsevier; 2015. Chapter 4; p. 345–435.
[30] Taylor MA, Bowen WP. Quantum metrology and its application in biology. Phys Rep. 2016;615:1–59.
[31] Pirandola S, Bardhan BR, Gehring T, et al. Advances in photonic quantum sensing. Nat Photonics. 2018;12:724.
[32] Moreau P-A, Toninelli E, Gregory T, et al. Imaging with quantum states of light. Nat Rev Phys. 2019;1:367–380.
[33] Fabre C, Treps N. Modes and states in quantum optics. 2019. arXiv:1912.09321 [quant-ph].
[34] Betzig E. Nobel lecture: single molecules, cells, and super-resolution optics. Rev Mod Phys. 2015;87:1153–1168.
[35] Pendry JB. Negative refraction. Contemp Phys. 2004;45:191–202.
[36] Moerner WE. Nobel lecture: single-molecule spectroscopy, imaging, and photocontrol: foundations for super-resolution microscopy. Rev Mod Phys. 2015;87:1183–1212.
[37] Hell SW. Nobel lecture: nanoscopy with freely propagating light. Rev Mod Phys. 2015;87:1169–1181.
[38] Tsang M, Nair R, Lu X-M. Quantum theory of superresolution for two incoherent optical point sources. Phys Rev X. 2016;6:031033.
[39] Tsang M. Subdiffraction incoherent optical imaging via spatial-mode demultiplexing. New J Phys. 2017;19:023054.
[40] Tsang M. Subdiffraction incoherent optical imaging via spatial-mode demultiplexing: semiclassical treatment. Phys Rev A. 2018;97:023830.
[41] Dutton Z, Kerviche R, Ashok A, et al. Attaining the quantum limit of superresolution in imaging an object's length via predetection spatial-mode sorting. Phys Rev A. 2019;99:033847.
[42] Tsang M. Quantum limit to subdiffraction incoherent optical imaging. Phys Rev A. 2019;99:012305.
[43] Zhou S, Jiang L. Modern description of Rayleigh's criterion. Phys Rev A. 2019;99:013808.
[44] Tsang M. Semiparametric estimation for incoherent optical imaging. Phys Rev Res. 2019;1:033006.
[45] Bonsma-Fisher KAG, Tham W-K, Ferretti H, et al. Realistic sub-Rayleigh imaging with phase-sensitive measurements. New J Phys. 2019;21:093010.
[46] Nair R, Tsang M. Interferometric superlocalization of two incoherent optical point sources. Opt Express. 2016;24:3684–3701.
[47] Tsang M, Nair R, Lu X-M. Quantum information for semiclassical optics. Proceedings of the SPIE, Quantum and Nonlinear Optics IV. Vol. 10029. Bellingham (WA): SPIE; 2016. p. 1002903.
[48] Nair R, Tsang M. Far-field superresolution of thermal electromagnetic sources at the quantum limit. Phys Rev Lett. 2016;117:190801.
[49] Lupo C, Pirandola S. Ultimate precision bound of quantum and subwavelength imaging. Phys Rev Lett. 2016;117:190802.
[50] Tsang M. Conservative classical and quantum resolution limits for incoherent imaging. J Mod Opt. 2018;65:1385–1391.
[51] Ang SZ, Nair R, Tsang M. Quantum limit for two-dimensional resolution of two incoherent optical point sources. Phys Rev A. 2017;95:063847.
[52] Lu X-M, Krovi H, Nair R, et al. Quantum-optimal detection of one-versus-two incoherent optical sources with arbitrary separation. NPJ Quant Inform. 2018;4:64.

[53] Řeháček J, Paúr M, Stoklasa B, et al. Optimal measurements for resolution beyond the Rayleigh limit. Opt Lett. 2017;42:231–234.
[54] Yang F, Nair R, Tsang M, et al. Fisher information for far-field linear optical superresolution via homodyne or heterodyne detection in a higher-order local oscillator mode. Phys Rev A. 2017;96:063829.
[55] Kerviche R, Guha S, Ashok A. Fundamental limit of resolving two point sources limited by an arbitrary point spread function. 2017 IEEE International Symposium on Information Theory (ISIT). Aachen, Germany: IEEE; 2017. p. 441–445.
[56] Chrostowski A, Demkowicz-Dobrzański R, Jarzyna M, et al. On super-resolution imaging as a multiparameter estimation problem. Int J Quant Inform. 2017;15:1740005.
[57] Řeháček J, Hradil Z, Stoklasa B, et al. Multiparameter quantum metrology of incoherent point sources: towards realistic superresolution. Phys Rev A. 2017;96:062107.
[58] Řeháček J, Hradil Z, Koutný D, et al. Optimal measurements for quantum spatial superresolution. Phys Rev A. 2018;98:012103.
[59] Backlund MP, Shechtman Y, Walsworth RL. Fundamental precision bounds for three-dimensional optical localization microscopy with Poisson statistics. Phys Rev Lett. 2018;121:023904.
[60] Napoli C, Piano S, Leach R, et al. Towards superresolution surface metrology: quantum estimation of angular and axial separations. Phys Rev Lett. 2019;122:140505.
[61] Yu Z, Prasad S. Quantum limited superresolution of an incoherent source pair in three dimensions. Phys Rev Lett. 2018;121:180504.
[62] Prasad S, Yu Z. Quantum-limited superlocalization and superresolution of a source pair in three dimensions. Phys Rev A. 2019;99:022116.
[63] Prasad S. Quantum limited super-resolution of an unequal-brightness source pair in three dimensions. 2019. arXiv:1908.10949 [quant-ph].
[64] Larson W, Saleh BEA. Resurgence of Rayleigh's curse in the presence of partial coherence. Optica. 2018;5:1382–1389.
[65] Tsang M, Nair R. Resurgence of Rayleigh's curse in the presence of partial coherence: comment. Optica. 2019;6:400–401.
[66] Larson W, Saleh BEA. Resurgence of Rayleigh's curse in the presence of partial coherence: reply. Optica. 2019;6:402–403.
[67] Grace MR, Dutton Z, Ashok A, et al. Approaching quantum limited super-resolution imaging without prior knowledge of the object location. 2019. arXiv:1908.01996 [physics, physics:quant-ph].
[68] Bisketzi E, Branford D, Datta A. Quantum limits of localisation microscopy. New J Phys. 2019;21:123032.
[69] Lupo C, Huang Z, Kok P. The quantum limit to incoherent imaging is achieved by linear interferometry. 2019. arXiv:1909.09581 [quant-ph].
[70] Lee KK, Ashok A. Surpassing Rayleigh limit: fisher information analysis of partially coherent source(s). Proceedings of the SPIE, Optics and Photonics for Information Processing XIII; San Diego, CA. Vol. 11136; 2019. p. 111360H.
[71] Gefen T, Rotem A, Retzker A. Overcoming resolution limits with quantum sensing. Nat Commun. 2019;10:1–9.
[72] Hradil Z, Řeháček J, Sánchez-Soto L, et al. Quantum Fisher information with coherence. Optica. 2019;6:1437–1440.
[73] Len YL, Datta C, Parniak M, et al. Resolution limits of spatial mode demultiplexing with noisy detection. Int J Quant Inform. 2019;17:1941015. doi:10.1142/S0219749919410156
[74] Lupo C. Subwavelength quantum imaging with noisy detectors. Phys Rev A. 2020;101:022323.
[75] Tang ZS, Durak K, Ling A. Fault-tolerant and finite-error localization for point emitters within the diffraction limit. Opt Express. 2016;24:22004.
[76] Tham W-K, Ferretti H, Steinberg AM. Beating Rayleigh's curse by imaging using phase information. Phys Rev Lett. 2017;118:070801.
[77] Paúr M, Stoklasa B, Hradil Z, et al. Achieving the ultimate optical resolution. Optica. 2016;3:1144.
[78] Yang F, Tashchilina A, Moiseev ES, et al. Far-field linear optical superresolution via heterodyne detection in a higher-order local oscillator mode. Optica. 2016;3:1148.
[79] Donohue JM, Ansari V, Řeháček J, et al. Quantum-limited time-frequency estimation through mode-selective photon measurement. Phys Rev Lett. 2018;121:090501.
[80] Parniak M, Borówka S, Boroszko K, et al. Beating the Rayleigh limit using two-photon interference. Phys Rev Lett. 2018;121:250503.
[81] Paúr M, Stoklasa B, Grover J, et al. Tempering Rayleigh's curse with PSF shaping. Optica. 2018;5:1177–1180.
[82] Hassett J, Malhorta T, Alonso MA, et al. Sub-Rayleigh limit localization with a spatial mode analyzer. Frontiers in optics/laser science, osa technical digest. Washington (DC): Optical Society of America; 2018. p. JW4A.124.
[83] Zhou Y, Yang J, Hassett JD, et al. Quantum-limited estimation of the axial separation of two incoherent point sources. Optica. 2019;6:534–541.
[84] Paúr M, Stoklasa B, Koutný D, et al. Reading out Fisher information from the zeros of the point spread function. Opt Lett. 2019;44:3114–3117.
[85] Wadood SA, Allen J, Zhou Y, et al. Superresolution using parity sorting with partially coherent light. Frontiers in Optics + Laser Science APS/DLS; 2019; Paper FM3C.7. Washington (DC): Optical Society of America; 2019. p. FM3C.7.
[86] Řeháček J, Paúr M, Stoklasa B, et al. Intensity-based axial localization at the quantum limit. Phys Rev Lett. 2019;123:193601.
[87] Lehmann EL, Casella G. Theory of point estimation. New York: Springer; 1998.
[88] Goodman JW. Introduction to Fourier optics. New York: McGraw-Hill; 2004.
[89] Goodman JW. Statistical optics. New York: Wiley; 1985.
[90] Pawley JB, editor. Handbook of biological confocal microscopy. New York: Springer; 2006.
[91] Nagaoka H. A new approach to Cramér-Rao bounds for quantum state estimation. IEICE; 1989. p. 9–14. (Tech.

rep.; IT 89-42); Reprinted in Hayashi M, editor. Asymptotic theory of quantum statistical inference. Singapore: World Scientific; 2005. Chapter 8; p. 100–112.
[92] Braunstein SL, Caves CM. Statistical distance and the geometry of quantum states. Phys Rev Lett. 1994;72:3439–3443.
[93] Hayashi M, editor. Asymptotic theory of quantum statistical inference: selected papers. Singapore: World Scientific; 2005.
[94] Fujiwara A. Strong consistency and asymptotic efficiency for adaptive quantum estimation problems. J Phys A. 2006;39:12489.
[95] Yuen HP, Shapiro JH. Optical communication with two-photon coherent states–Part I: quantum-state propagation and quantum-noise. IEEE Trans Inform Theory. 1978;24:657–668.
[96] Snyder DL, Miller MI. Random point processes in time and space. New York: Springer-Verlag; 1991.
[97] Tsang M. Quantum limits to optical point-source localization. Optica. 2015;2:646–653.
[98] Morizur J-F, Nicholls L, Jian P, et al. Programmable unitary spatial mode manipulation. J Opt Soc Am A. 2010;27:2524–2531.
[99] Roddier F. Interferometric imaging in optical astronomy. Phys Rep. 1988;170:97–166.
[100] Wicker K, Heintzmann R. Interferometric resolution improvement for confocal microscopes. Opt Express. 2007;15:12206.
[101] Wicker K, Sindbert S, Heintzmann R. Characterisation of a resolution enhancing image inversion interferometer. Opt Express. 2009;17:15491.
[102] Weigel D, Foerster R, Babovsky H, et al. Enhanced resolution of microscopic objects by image inversion interferometry. Opt Express. 2011;19:26451.
[103] Weigel D, Babovsky H, Kiessling A, et al. Investigation of the resolution ability of an image inversion interferometer. Opt Commun. 2011;284:2273–2277.
[104] Larson W, Tabiryan NV, Saleh BEA. A common-path polarization-based image-inversion interferometer. Opt Express. 2019;27:5685–5695.
[105] Xue X, Wei H, Kirk AG. Beam analysis by fractional Fourier transform. Opt Lett. 2001;26:1746–1748.
[106] Abouraddy AF, Yarnall TM, Saleh BEA. Generalized optical interferometry for modal analysis in arbitrary degrees of freedom. Opt Lett. 2012;37:2889–2891.
[107] Martin L, Mardani D, Kondakci HE, et al. Basis-neutral Hilbert-space analyzers. Sci Rep. 2017;7:44995.
[108] Lohmann AW, Mendlovic D, Zalevsky Z. Fractional transformations in optics. In: Wolf E, editor. Progress in optics. Vol. 38. Amsterdam: Elsevier; 1998. Chapter IV; p. 263–342.
[109] Wolter H. Untersuchungen zur Strahlversetzung bei Totalreflexion des Lichtes mit der Methode der Minimumstrahlkennzeichnung. Z Naturforsc A. 1950;5:143–153.
[110] Forbes A, Dudley A, McLaren M. Creation and detection of optical modes with spatial light modulators. Adv Opt Photonics. 2016;8:200–227.
[111] Townes CH. Noise and sensitivity in interferometry. In: Lawson PR, editor. Principles of long baseline stellar interferometry. Pasadena: Jet Propulsion Laboratory; 2000. Chapter 4; p. 59–70.
[112] Tsang M. Quantum nonlocality in weak-thermal-light interferometry. Phys Rev Lett. 2011;107:270402.
[113] Eckstein A, Brecht B, Silberhorn C. A quantum pulse gate based on spectrally engineered sum frequency generation. Opt Express. 2011;19:13770–13778.
[114] Debnath L, Mikusiński P. Introduction to Hilbert spaces with applications. Amsterdam: Elsevier; 2005.
[115] Dunkl CF, Xu Y. Orthogonal polynomials of several variables. Cambridge: Cambridge University Press; 2014.
[116] Hayashi M. Quantum information theory: mathematical foundation. Berlin: Springer; 2017.
[117] Ng S, Ang SZ, Wheatley TA, et al. Spectrum analysis with quantum dynamical systems. Phys Rev A. 2016;93:042121.
[118] Huang F, Schwartz SL, Byars JM, et al. Simultaneous multiple-emitter fitting for single molecule super-resolution imaging. Biomed Opt Express. 2011;2:1377–1393.
[119] Van Trees HL. Detection, estimation, and modulation theory, part I. New York: John Wiley & Sons; 2001.
[120] Labeyrie A, Lipson SG, Nisenson P. An introduction to optical stellar interferometry. Cambridge: Cambridge University Press; 2006.
[121] Pearce ME, Campbell ET, Kok P. Optimal quantum metrology of distant black bodies. Quantum. 2017;1:21.
[122] Howard LA, Gillett GG, Pearce ME, et al. Optimal imaging of remote bodies using quantum detectors. Phys Rev Lett. 2019;123:143604.
[123] Davis J, Tango WJ. New determination of the angular diameter of Sirius. Nature. 1986;323:234–235.
[124] Genovese M. Real applications of quantum imaging. J Opt. 2016;18:073002.
[125] Schneider R, Mehringer T, Mercurio G, et al. Quantum imaging with incoherently scattered light from a free-electron laser. Nat Phys. 2018;14:126–129.
[126] Tenne R, Rossman U, Rephael B, et al. Super-resolution enhancement by quantum image scanning microscopy. Nat Photonics. 2019;13:116.
[127] Berchera IR, Degiovanni IP. Quantum imaging with sub-Poissonian light: challenges and perspectives in optical metrology. Metrologia. 2019;56:024001.
[128] Khurgin JB. How to deal with the loss in plasmonics and metamaterials. Nat Nanotechnol. 2015;10:2–6.
[129] Tan S-H, Erkmen BI, Giovannetti V, et al. Quantum illumination with Gaussian states. Phys Rev Lett. 2008;101:253601.
[130] Dowling JP, Milburn GJ. Quantum technology: the second quantum revolution. Philos Trans Roy Soc London A. 2003;361:1655–1674.
[131] Gottesman D, Jennewein T, Croke S. Longer-baseline telescopes using quantum repeaters. Phys Rev Lett. 2012;109:070503.
[132] Khabiboulline ET, Borregaard J, De Greve K, et al. Optical interferometry with quantum networks. Phys Rev Lett. 2019;123:070504.
[133] Rogers ETF, Zheludev NI. Optical super-oscillations: sub-wavelength light focusing and super-resolution imaging. J Opt. 2013;15:094008.
[134] Kellerer AN, Ribak EN. Beyond the diffraction limit via optical amplification. Opt Lett. 2016;41:3181–3184.

[135] Rafsanjani SMH, Mirhosseini M, Loaiza OSM, et al. Quantum-enhanced interferometry with weak thermal light. Optica. 2017;4:487–491.
[136] Prasad S. Implications of light amplification for astronomical imaging. J Opt Soc Am A. 1994;11:2799–2803.
[137] Lantz E. Quantum-enhanced interferometry with weak thermal light: comment. Optica. 2017;4:1314–1316.
[138] Esposito S, Riccardi A, Pinna E, et al. Large binocular telescope adaptive optics system: new achievements and perspectives in adaptive optics. Proceedings of the SPIE, Astronomical Adaptive Optics Systems and Applications IV. Vol. 8149. Bellingham (WA): SPIE; 2011. p. 814902.
[139] Michalet X, Colyer RA, Scalia G, et al. Development of new photon-counting detectors for single-molecule fluorescence microscopy. Philos Trans Roy Soc B. 2013;368:20120035.
[140] Glauber RJ. Nobel lecture: one hundred years of light quanta. Rev Mod Phys. 2006;78:1267–1278.
[141] Horn RA, Johnson CR. Matrix analysis. Cambridge: Cambridge University Press; 1985.

Appendices

Appendix 1. Cramér-Rao bound and Fisher information

Let $\{P_Y(y\,|\,\theta) > 0 : y \in \Omega, \theta \in \Theta \subseteq \mathbb{R}\}$ be a family of probability distributions for an observed random variable Y, where θ is an unknown scalar parameter and the support Ω is assumed to be countable and common to all distributions for simplicity. Let $\check{\theta}(Y)$ be an estimator of θ. Define the mean-square error as

$$\mathrm{MSE}(\theta) \equiv \mathbb{E}\left[\check{\theta}(Y) - \theta\right]^2 = \sum_y P_Y(y\,|\,\theta)\left[\check{\theta}(y) - \theta\right]^2, \tag{A1}$$

where $\mathbb{E}$ denotes the expectation. The unbiased condition is

$$\mathbb{E}\left[\check{\theta}(Y)\right] = \theta. \tag{A2}$$

Under certain regularity conditions on the distributions, the Cramér-Rao bound given by Equation (1) holds for any unbiased estimator, where the Fisher information is [87]

$$\mathrm{FI}(\theta) \equiv \sum_y \frac{1}{P_Y(y\,|\,\theta)}\left[\frac{\partial P_Y(y\,|\,\theta)}{\partial\theta}\right]^2. \tag{A3}$$

Generalization for probability densities is straightforward [87].

Appendix 2. Helstrom information

Let $\{\rho(\theta) : \theta \in \Theta \subseteq \mathbb{R}\}$ be a family of density operators for a quantum object. Under a quantum measurement, the generalised Born's rule is given by

$$P_Y(y\,|\,\theta) = \mathrm{tr}E_Y(y)\rho(\theta), \tag{A4}$$

where tr denotes the operator trace and $E_Y(y)$ is called the positive operator-valued measure (POVM), which models the measurement statistics [116]. Define the Helstrom information as [24]

$$\mathrm{HI} = \mathrm{tr}\rho L^2 = \mathrm{tr}\frac{\partial\rho}{\partial\theta}L, \tag{A5}$$

where L is a solution to

$$\frac{\partial\rho}{\partial\theta} = \frac{1}{2}(\rho L + L\rho). \tag{A6}$$

For any POVM, Helstrom proved $\mathrm{MSE} \geq \mathrm{HI}^{-1}$ [24], while Nagaoka [91] and Braunstein and Caves [92] proved

$$\mathrm{FI}(\theta) \leq \mathrm{HI}(\theta). \tag{A7}$$

Although they also proved that $\max_{E_Y}\mathrm{FI}(\theta) = \mathrm{HI}(\theta)$ and a projection in the eigenstates of L gives an optimal POVM, it is important to keep in mind that L is a function of θ, and the optimal POVM derived from it at one value of θ may be suboptimal at other values. In practice, obviously θ is unknown, and there is no guarantee that one can find a POVM that is optimal across a range of θ. A solution, proposed by Nagaoka and refined by Hayashi and Matsumoto [93] and Fujiwara [94], is to consider repeated adaptive measurements, and they showed that the total Fisher information of such measurements can approach the Helstrom information in the limit of infinitely many measurements under certain technical conditions.

Appendix 3. Thermal state in the ultraviolet limit

Consider thermal light in one temporal mode and multiple spatial modes, and let $\{a_0, a_1, \ldots\}$ be the annihilation operators for the spatial modes. As first proposed by Glauber [140], the thermal state is [24]

$$\sigma = \mathbb{E}\left(|\alpha\rangle\langle\alpha|\right) = \int \mathrm{d}^2\alpha\,\Phi(\alpha)\,|\alpha\rangle\langle\alpha|, \tag{A8}$$

$$\Phi(\alpha) = \frac{1}{\det(\pi\Gamma)}\exp\left(-\alpha^\dagger\Gamma^{-1}\alpha\right), \tag{A9}$$

where $\alpha = (\alpha_0, \alpha_1, \ldots)^\top$ is a column vector of zero-mean complex Gaussian random variables with probability density Φ, $\top$ denotes the transpose, † denotes the conjugate transpose, $|\alpha\rangle$ is a multimode coherent state that obeys $a_q|\alpha\rangle = \alpha_q|\alpha\rangle$, and Γ is the mutual coherence matrix [3]. In particular, the first moments of α are given by

$$\mathbb{E}(\alpha) = 0, \quad \mathbb{E}(\alpha\alpha^\top) = 0, \quad \mathbb{E}(\alpha\alpha^\dagger) = \Gamma. \tag{A10}$$

The photon-counting distribution is

$$P(n) = \langle n|\,\sigma\,|n\rangle = \mathbb{E}\,|\langle n\,|\,\alpha\rangle|^2, \tag{A11}$$

$$|n\rangle = \prod_q \frac{(a_q^\dagger)^{n_q}}{\sqrt{n_q!}}\,|\mathrm{vac}\rangle, \tag{A12}$$

$$|\langle n\,|\,\alpha\rangle|^2 = \exp(-\alpha^\dagger\alpha)\prod_q \frac{|\alpha_q|^{2n_q}}{n_q!}, \tag{A13}$$

where $|n\rangle$ is a Fock state and $|\mathrm{vac}\rangle$ is the vacuum state. Equation (A11) agrees with the semiclassical theory by Mandel [3]. With M temporal modes, the density operator can be modelled as M copies of σ, or

$$\rho = \sigma^{\otimes M}. \tag{A14}$$

To simplify the thermal state for optical frequencies, let

$$\epsilon \equiv \mathrm{tr}\Gamma \tag{A15}$$

be the average photon number per temporal mode and

$$g \equiv \frac{\Gamma}{\mathrm{tr}\Gamma} \tag{A16}$$

be the normalised mutual coherence matrix. Define the ultraviolet limit as $\epsilon \to 0$ while holding $N = M\epsilon$ constant. The zero-photon probability per temporal mode is

$$P(0,\ldots,0) = \mathbb{E}\left[\exp(-\alpha^\dagger\alpha)\right] = 1 - \epsilon + O(\epsilon^2), \quad \text{(A17)}$$

the one-photon probability is

$$P(0,\ldots,n_q=1,0,\ldots) = \mathbb{E}\left[\exp(-\alpha^\dagger\alpha)|\alpha_q|^2\right] = \epsilon g_q + O(\epsilon^2), \quad \text{(A18)}$$

where the diagonal entries of a matrix are abbreviated as $g_{qq} = g_q$, and the probability of two or more photons is $O(\epsilon^2)$. The photon counts summed over M temporal modes hence become Poisson in the ultraviolet limit [89]. A simplified quantum model in this limit is [38,112]

$$\sigma = (1-\epsilon)\,|\text{vac}\rangle\langle\text{vac}| + \epsilon\rho_1 + O(\epsilon^2), \quad \text{(A19)}$$

where the one-photon density operator is

$$\rho_1 = \sum_{q,p} g_{qp}\,|\phi_q\rangle\langle\phi_p|\,, \quad |\phi_q\rangle = a_q^\dagger\,|\text{vac}\rangle\,. \quad \text{(A20)}$$

For paraxial incoherent imaging in particular [39],

$$\rho_1 = \int_{-\infty}^{\infty} \mathrm{d}X F(X)\,\mathrm{e}^{-i\hat{k}X}\,|\psi\rangle\langle\psi|\,\mathrm{e}^{i\hat{k}X}, \quad \text{(A21)}$$

where $\hat{k}$ is the spatial-frequency or momentum operator, $|\psi\rangle$ is the one-photon state with spatial wavefunction $\langle x\,|\,\psi\rangle = \psi(x)$, and $|x\rangle$ is the one-photon position eigenket that obeys $\langle x\,|\,x'\rangle = \delta(x-x')$. $f(x) = \langle x|\,\rho_1\,|x\rangle$ gives Equation (7), while $g_q = \langle\phi_q|\,\rho_1\,|\phi_q\rangle$ gives Equation (8). If f and g depend on θ (but ϵ does not), the Fisher information for the Poisson processes is given by Equations (10) and (12).

The ultraviolet limit and the negligence of $O(\epsilon^2)$ terms mean that multiphoton coincidence events and bunching effects are ignored [89]. Besides thermal sources, the model here also applies to any incoherent sources, such as fluorescent sources [90] or even electrons [8,9], as long as they obey an incoherent-imaging model with Poisson counting statistics.

For the thermal state given by Equations (A8) and (A9), Helstrom showed that [24]

$$\mathrm{HI} = \mathrm{tr}\frac{\partial\Gamma}{\partial\theta}\Upsilon, \quad \text{(A22)}$$

where Υ is a solution to

$$\frac{\partial\Gamma}{\partial\theta} = \frac{1}{2}\left[\Gamma\Upsilon(I+\Gamma) + (I+\Gamma)\Upsilon\Gamma\right], \quad \text{(A23)}$$

and I is the identity matrix. Reference [42, Appendix A] shows that the information given by Equations (A22) and (A23) on a per-photon basis is upper-bounded by its ultraviolet limit, which coincides with the information computed for the one-photon density operator ρ_1 given by Equation (A20) if ϵ does not depend on θ, viz.,

$$\frac{\mathrm{HI}^{(\sigma)}}{\epsilon} \le \lim_{\epsilon\to 0}\frac{\mathrm{HI}^{(\sigma)}}{\epsilon} = \mathrm{HI}^{(\rho_1)}. \quad \text{(A24)}$$

With M temporal modes, the Helstrom bound is multiplied by M [116], so $\mathrm{HI}^{(\rho)} = M\mathrm{HI}^{(\sigma)}$, and the total information in the ultraviolet limit becomes

$$\mathrm{HI}^{(\rho)} \le \lim_{\epsilon\to 0}\mathrm{HI}^{(\rho)} = N\mathrm{HI}^{(\rho_1)}, \quad \text{(A25)}$$

which means that $\mathrm{HI}^{(\rho_1)}$ also serves as a limit for thermal states with arbitrary ϵ if ϵ does not depend on θ.

If ϵ depends on θ, which may happen with partially coherent sources [65], one must be more careful and go back to Equations (A22) and (A23). For $\epsilon \ll 1$, $I + \Gamma \approx I$, and Equation (A23) can be approximated as

$$\frac{\partial\Gamma}{\partial\theta} \approx \frac{1}{2}\left(\Gamma\Upsilon + \Upsilon\Gamma\right). \quad \text{(A26)}$$

Equations (A22) and (A26), in terms of the mutual coherence matrix Γ, resemble Equations (A5) and (A6) in terms of the density operator ρ. Notice, however, that Equations (A22) and (A26) are in terms of the *unnormalized* Γ. References [64,72], on the other hand, use the normalised version $g = \Gamma/\mathrm{tr}\Gamma$ in the formulas and may have produced unphysical results for partially coherent sources.

Appendix 4. Gram-Schmidt process

Consider an inner-product space equipped with an inner product $\langle u, v\rangle$ between two elements u and v and a norm $\|u\| = \sqrt{\langle u, u\rangle}$. An illustrative example is the space of Euclidean vectors in $\mathbb{R}^d$, with the dot product as the inner product and the vector length as the norm. Given a set of linearly independent elements $S = \{u_0, u_1, \ldots\}$, the Gram-Schmidt process produces an orthonormal basis $\{b_0, b_1, \ldots\}$ for the space spanned by S [114]. The process starts with

$$v_0 = u_0, \quad b_0 = \frac{v_0}{\|v_0\|}. \quad \text{(A27)}$$

Then, for each $q = 1, 2, \ldots,$

$$v_q = u_q - \sum_{p=0}^{q-1}\langle u_q, b_p\rangle\, b_p, \quad b_q = \frac{v_q}{\|v_q\|}. \quad \text{(A28)}$$

$\|b_q\| = \sqrt{\langle b_q, b_q\rangle} = 1$ by design. One can check that v_q and b_q are orthogonal to $\{b_0, \ldots, b_{q-1}\}$. It follows that $\{b_0, \ldots, b_q\}$ is an orthonormal basis with

$$\langle b_q, b_p\rangle = \delta_{qp}. \quad \text{(A29)}$$

Since the space spanned by $\{b_0, \ldots, b_{q-1}\}$ is the same as the space spanned by $\{u_0, \ldots, u_{q-1}\}$, each b_q is also orthogonal to $\{u_0, \ldots, u_{q-1}\}$.

Appendix 5. Multiparameter estimation

Now suppose that $\theta \in \Theta \subseteq \mathbb{R}^K$ is a column vector of parameters, and the estimator is also a vector. Define the mean-square error covariance matrix as

$$\mathrm{MSE}_{\mu\nu}(\theta) \equiv \mathbb{E}\left[\check{\theta}_\mu(Y) - \theta_\mu\right]\left[\check{\theta}_\nu(Y) - \theta_\nu\right]. \quad \text{(A30)}$$

Diagonal entries of a matrix are again abbreviated as $\mathrm{MSE}_{\mu\mu} = \mathrm{MSE}_\mu$. The multiparameter Cramér-Rao bound [87] can be expressed as the matrix inequality

$$\mathrm{MSE} \ge \mathrm{CRB} \equiv \mathrm{FI}^{-1}, \quad \text{(A31)}$$

$$\mathrm{FI}_{\mu\nu}(\theta) \equiv \sum_y \frac{1}{P_Y(y\,|\,\theta)}\frac{\partial P_Y(y\,|\,\theta)}{\partial\theta_\mu}\frac{\partial P_Y(y\,|\,\theta)}{\partial\theta_\nu}. \quad \text{(A32)}$$

The matrix inequality means that MSE − CRB is positive-semidefinite [141], or equivalently $u^\top(\mathrm{MSE}-\mathrm{CRB})u \geq 0$ for any real column vector u. For example, the multiparameter Cramér-Rao bounds for two point sources and more general objects measured with direct imaging and SPADE have been derived in Refs. [38–40,44,51].

The Helstrom information matrix is defined as

$$\mathrm{HI}_{\mu\nu} \equiv \mathrm{Re}\mathrm{tr}\rho L_\mu L_\nu = \mathrm{tr}\frac{\partial\rho}{\partial\theta_\mu}L_\nu, \tag{A33}$$

$$\frac{\partial\rho}{\partial\theta_\mu} = \frac{1}{2}\left(\rho L_\mu + L_\mu\rho\right). \tag{A34}$$

The matrices can be shown to inherit all the properties of their scalar version by substituting the directional derivative $\partial/\partial\theta = \sum_\mu u_\mu \partial/\partial\theta_\mu$ and $L = \sum_\mu u_\mu L_\mu$ for an arbitrary real vector u. For example, upon the substitutions, the scalar Fisher information becomes $u^\top \mathrm{FI} u$ and the scalar Helstrom information becomes

$$\mathrm{tr}\rho L^2 = u^\top \mathcal{H} u = u^\top \mathrm{HI} u, \quad \mathcal{H}_{\mu\nu} \equiv \mathrm{tr}\rho L_\mu L_\nu, \tag{A35}$$

where I have used the fact that, since $u^\top\mathcal{H}u$ and u are real, $u^\top\mathcal{H}u = \mathrm{Re}(\sum_\mu u_\mu \mathcal{H}_{\mu\nu}u_\nu) = \sum_\mu u_\mu \mathrm{Re}(\mathcal{H}_{\mu\nu})u_\nu = \sum_\mu u_\mu \mathrm{HI}_{\mu\nu}u_\nu$. The Nagaoka bound given by Equation (A7) becomes $u^\top\mathrm{FI}u \leq u^\top\mathrm{HI}u$, meaning that Equation (A7) still holds as a matrix inequality. A consequence of the matrix inequality is that the inverses obey the reverse relation [141], so the Nagaoka bound leads to

$$\mathrm{MSE} \geq \mathrm{FI}^{-1} \geq \mathrm{HI}^{-1}. \tag{A36}$$